Direct Synthesis of $LiNi_{1/3}Co_{1/3}Mn_{1/3}O_2$ from Nitrate Precursors

Sébastien Patoux and Marca M. Doeff

Materials Sciences Division

Lawrence Berkeley National Laboratory

University of California

Berkeley, CA 94720, USA

Acknowledgments

This work was supported by the Assistant Secretary for Energy Efficiency and Renewable Energy, Office of FreedomCAR and Vehicle Technologies of the U.S. Department of Energy under Contract No. DE-AC03-76SF00098. We would like to thank Tanaka Chemical Corporation (Osaka, Japan) for their gift of $LiNi_{1/3}Co_{1/3}Mn_{1/3}O_2$.

Abstract

Two novel methods for synthesis of the title compound directly from metal nitrates are described. Phase-pure materials are produced when precursors are calcined between 600 and 1000°C, with little to no ion mixing exhibited for products heated to 900°C or above. The electrochemical characteristics of these materials depended upon calcination temperature and synthesis method, with results comparable to a commercial sample for the materials made at high temperatures in a one-step process without combustion. The sample prepared by combustion also exhibited very stable capacity retention upon cycling.

Keywords: Lithium batteries; lithium nickel manganese cobalt oxides; layered cathodes

Introduction

Recently, intensive effort has been directed towards development of $LiNi_{1/2}Mn_{1/2}O_2$ [1, 2, 3], $LiNi_{1/3}Co_{1/3}Mn_{1/3}O_2$ [4, 5], and variants [6, 7] as possible replacements for $LiCoO_2$ positive electrodes in Li ion batteries. Computational [8, 9, 10] and spectroscopic studies [11] show that, under normal cycling conditions, Mn remains in the +4 oxidation state, thus avoiding complications associated with the Jahn-Teller distortion of Mn^{3+} ions in six-coordinate sites. These materials exhibit slightly sloping discharge profiles. The capacities obtained are dependent upon composition and voltage limits, with 200 mAh/g reported for $LiNi_{1/3}Co_{1/3}Mn_{1/3}O_2$ when cells with lithium anodes are charged to 4.6V [4]. Ion mixing [12] (i.e., Ni in Li sites and *vice versa*) can reduce the effective capacity and adversely affect rate capability, and is more likely to

occur when Ni contents are relatively high. Cobalt is electro-active in these compounds and may replace some of the Ni, reducing this tendency [13] and improving rate capability [14].

$LiNi_{1/3}Co_{1/3}Mn_{1/3}O_2$ is usually synthesized by the mixed hydroxide method [15], in which a $M(OH)_2$ (M = Ni, Co, Mn) precursor is precipitated from a metal nitrate solution and is then reacted with a lithium salt at elevated temperature. This is not difficult in practice, but pH, temperature, flow conditions, concentrations, and other factors influence the crystal structure, purity, and physical properties of the products, and must be carefully controlled for optimum electrochemical performance [16]. Unfortunately, this synthetic procedure is difficult to modify for fabrication of the thin films necessary for electrochemical studies. Our intention in this study was to determine alternative synthesis routes that could be adapted for this purpose. Herein, we describe direct synthesis from metal nitrates that result in phase-pure materials with good electrochemical behavior.

Experimental

$LiNi_{1/3}Co_{1/3}Mn_{1/3}O_2$ was synthesized by two different methods. For the sample designated GNC, glycine-nitrate combustion [17, 18] was used. An aqueous solution of $LiNO_3$, $Ni(NO_3)_2{\cdot}6H_2O$, $Co(NO_3)_2{\cdot}6H_2O$ and $Mn(NO_3)_2$ in HNO_3, in proportion to give $LiNi_{1/3}Co_{1/3}Mn_{1/3}O_2$, was mixed with glycine in the molar ratio 1:2 (glycine:nitrate). The solution was combusted by evaporating small aliquots of solution to dryness until the desired amount of product was obtained. The temperature of the combustion reaction is determined by the glycine: nitrate ratio, which was chosen to give 1300-1400°C. The as-prepared dark-brown powder was then calcined at 800°C for 4h to remove any organic residue and to ensure better homogeneity.

Five other samples of $LiNi_{1/3}Co_{1/3}Mn_{1/3}O_2$ composition were synthesized from the same metal nitrates precursors, but without using glycine. For each of these samples, an aqueous solution was obtained by dissolving the metal nitrates in stoichiometric proportions in concentrations of approximately 0.43 mol. L^{-1} for Ni, Co and Mn, and 1.3 mol. L^{-1} for Li. The water was then slowly evaporated under stirring at 60-80°C on a hot plate. The temperature of the resulting viscous purple solution was then increased to approximately 120°C in order to partially remove the nitrate ions. After a few hours, the beaker was placed overnight in an oven at 120°C. The resulting solid was then ground in a mortar and annealed under air at temperatures ranging from 600 to 1000°C. One sample was first heated at 600°C and then at 1000°C. These samples are designated by the final calcination temperatures, 600°C, 700°C, 800°C, 900°C and 1000°C. The reaction times within the furnace were arbitrary chosen to be 16, 14, 12, 10 and 8h, respectively. A commercial sample of $LiNi_{1/3}Co_{1/3}Mn_{1/3}O_2$ (Lot # LNCMO 30301) was obtained as a gift from Tanaka Chemical Corporation (Osaka, Japan) and was tested for comparison purposes.

X-ray diffraction (XRD) patterns at 300K were obtained on a Philips X'Pert diffractometer (θ-θ geometry, back monochromator) using CuK_α radiation. Lattice parameters were determined by Full Pattern Matching using the WinPLOTR/Fullprof suite [19]. The Scherrer equation [20] was used to estimate the average crystallite sizes. Here, we assumed that the broadening of the diffraction peaks was mainly dominated by the crystallite size effect, and there was negligible contribution from microstrain. Values in Table 1 were determined using a Thompson-Cox-Hastings profile function (the calculated values are somewhat dependent upon the definition used for peak broadening, although the observed trends remain the same).

Composite positive electrodes were prepared by thoroughly mixing the active material (84%) with carbon black (4%), SFG-6 graphite (4%) and polyvinylidene fluoride-Kynar 741 (8%) in N-

methyl-pyrrolidone and extruding onto aluminum foils. Electrodes, with loadings between 8 and 10 mg of active material/cm^2 were dried for 24h at room temperature and then for 24h at 100-120°C under vacuum. 2032 coin cells were then assembled in a helium filled dry box (< 1ppm O_2/H_2O) using foils of Li metal as counter electrodes and Celgard 3401 saturated with a 1 M $LiPF_6$ (electrolyte) in ethylene carbonate/dimethylcarbonate (1:2 in weight) as separators. Several coin cells containing each sample were assembled and tested, to ensure reproducibility. Lithium insertion/extraction was monitored with an Arbin BT/HSP-2043 automatic cycling data recording system operating in galvanostatic mode.

Results and Discussion

Figure 1 shows XRD patterns of the $LiNi_{1/3}Co_{1/3}Mn_{1/3}O_2$ samples made directly from nitrates and by GNC, as well as that provided by Tanaka. All reflections in each of the patterns were unambiguously indexed with the space group $R\bar{3}m$, indicating that phase-pure materials are produced under all the conditions used for this study. Unit cell parameters, average crystallite sizes, and the ratios of the integrated intensities of the (003) and (104) peaks ($R_{003/104}$) are summarized in Table 1. For similar samples without preferred orientation, the latter is an approximate measure of the amount of ion mixing [21, 22]. Higher values of $R_{003/104}$ are desirable, although the theoretical ratio, corresponding to an ideal structure in which no Li in located in transition metal sites and *vice versa*, depends upon thermal factors, valences, composition, and other factors. Best results are obtained for the materials made directly from nitrates and calcined at 900-1000ºC, while those heated to temperatures below 900ºC and that made by GNC show some evidence of ion mixing.

The first cycles, between 4.3 and 2.5V, of representative lithium half-cells containing the various $LiNi_{1/3}Co_{1/3}Mn_{1/3}O_2$ samples are shown in Figure 2. All cells show coulombic inefficiencies; i.e., more capacity is observed upon charge than on discharge. For the series of materials made directly from nitrates, the irreversible capacities are inversely correlated with the crystallite size estimated from XRD peak broadening (Table 1), and decrease as the calcination temperature increases (except for 1000˚C). Somewhat surprisingly, the GNC sample did not follow this trend, exhibiting the lowest irreversible capacity, in spite of the small crystallite size. Careful observation of the cycling curves in Figure 2 indicates that the charge ended somewhat prematurely, due to the high overpotential of the cell (evident in the wide separation between the charge and discharge traces). While this minimizes the irreversible oxidation of the electrolytic solution, which is most likely the main source of the coulombic inefficiency in this potential range, it also lowers the subsequent discharge capacity somewhat (135 mAh/g). High overpotentials are also seen in the cells containing materials made at 800˚C or below, and may be attributable to rate limitations in the positive electrodes caused by ion mixing. In contrast, cells containing materials made at 900˚C and 1000˚C exhibit very low overpotentials and yielded the same discharge capacities as that containing the Tanaka sample (140-145 mAh/g), but with lower irreversible capacities.

The coulombic inefficiencies decreased markedly during the subsequent cycles of most cells. Capacity retention upon cycling between 4.3 and 2.5V was better for samples that initially exhibited little irreversibility (GNC, 900˚C, and 1000˚C, Figure 3). The latter two materials, in particular, show excellent cycling behavior, with both higher initial capacities and better capacity retention than other samples. Figure 4 shows discharges at various current densities for a cell containing 900˚C-$LiNi_{1/3}Co_{1/3}Mn_{1/3}O_2$. A tenfold increase in rate results in less than 10%

decrease in delivered capacity, similar to that found for the Tanaka-$LiNi_{1/3}Co_{1/3}Mn_{1/3}O_2$ (not shown).

$LiNi_{1/3}Co_{1/3}Mn_{1/3}O_2$ is only partially de-intercalated when cells are charged to 4.3V. Higher discharge capacities can be obtained when the voltage limit upon charge is raised. Figure 5 shows first cycles for cells containing 900˚C- $LiNi_{1/3}Co_{1/3}Mn_{1/3}O_2$ charged to 4.3, 4.5, or 4.7V. Although utilization is greater for cells charged to higher voltages, this comes at the expense of increased coulombic inefficiencies and more rapid capacity fading upon cycling (see inset). Venkatraman et al. [13] have shown that oxygen loss from layered metal oxide cathodes becomes significant above 4.25V vs. Li. This may contribute to the observed cycling losses and limits the achievable practical capacities that can be obtained, unless steps are taken to reduce oxygen activity. These approaches include coating particle surfaces with a protective material such as colloidal ZrO_2, which may bond to surface oxygen [23] or incorporating stabilizing components such as Li_2TiO_3 in the electrodes [24]. It should be noted, however, that other cell components such as current collectors might have to be protected or modified, if cells are cycled to higher potentials to take advantage of the additional capacity. Careful control of impurities (e.g., water) and optimization of both electrode and electrolytic solution compositions may minimize or eliminate entirely the irreversible oxidation of the latter, but oxidative intercalation of anions in graphite (used as a conductive additive in cathodes) at high potentials may still cause deterioration of cell performance [25]. If these issues can be addressed successfully, it should be possible to increase energy densities of Li-ion cells containing $LiNi_{1/3}Co_{1/3}Mn_{1/3}O_2$ or other layered oxide cathodes simply by charging them further than is currently feasible.

Conclusions

Phase-pure $LiNi_{1/3}Co_{1/3}Mn_{1/3}O_2$ samples were synthesized directly from nitrate precursors and by a glycine-nitrate combustion (GNC) process. Materials differed in the amount of ion mixing and the average crystallite size as determined from the X-ray powder diffraction data. These parameters directly influence the electrochemical behavior in lithium cells by affecting the depth of charge attainable, rate capabilities, the coulombic inefficiencies observed on the first cycle, and the capacity retention upon cycling. Results for $LiNi_{1/3}Co_{1/3}Mn_{1/3}O_2$ made directly from nitrates and heated to 900˚C or 1000˚C compared favorably to that of a commercial sample in terms of the irreversible capacity observed upon the first cycle and the cycling performance.

Acknowledgments

This work was supported by the Assistant Secretary for Energy Efficiency and Renewable Energy, Office of FreedomCAR and Vehicle Technologies of the U.S. Department of Energy under Contract No. DE-AC03-76SF00098. We would like to thank Tanaka Chemical Corporation (Osaka, Japan) for their gift of $LiNi_{1/3}Co_{1/3}Mn_{1/3}O_2$.

References

1. E. Rossen, C. D. W. Jones, and J.R. Dahn, Solid State Ionics 57 (1992) 311.

2. M. E. Spahr, P. Novák, B. Schynder, O. Haas, and R. Nesper, J. Electrochem. Soc. 145 (1998) 1113.

3. Y. Makimura and T. Ohzuku, J. Power Sources 119-121 (2003) 156.

4. N. Yabuuchi and T. Ohzuku, J. Power Sources 119-121 (2003) 171. ;

5. K.M. Shaju, G.V. Subba Rao and B.V.R. Chowdari, Electrochem. Acta 48 (2002) 145.

6. C. S. Johnson, J.-S. Kim, A. J. Kropf, A. J. Kahaian, J. T. Vaughey, and M. M. Thackeray, Electrochem. Commun. 4 (2002) 492.

7. Z. Lu, L. Y. Beaulieu, R.A. Donaberger, C. L. Thomas, and J. R. Dahn, J. Electrochem. Soc. 149 (2002) A778.

8. M. S. Islam, R. A. Davies, and J. D. Gale, Chem. Mater. 15 (2003) 4280.

9. B.J. Hwang, Y.W. Tsai, D. Carlier and G. Ceder, Chem. Mater. 15 (2003) 3676.

10. J. Reed and G. Ceder, Electrochem. and Sol. State Lett. 5 (2002) A145.

11. C. S. Johnson, J.-S. Kim, A. J. Kropf, A. J. Kahaian, J. T. Vaughey, L. M. L. Fransson, K. Edström, and M. M. Thackeray, Chem. Mater. 15 (2003) 2313.

12. W.-S. Yoon, Y. Paik, X-Q. Yang, M. Balasubramanian, J. McBreen and C.P. Grey, Electrochem. And Solid State Lett. 5 (2002) A263.

13. S. Venkatram and A. Manthiram, Chem. Mater. 15 (2003) 5003.

14. Y. Sun, C. Ouyang, Z. Wang, X. Huang, and L. Chen, J. Electrochem. Soc. 151 (2004) A504.

15. Y, Chen G. X. Wang, K. Konstantinov, H.K. Liu, and S. X. Dou, J. Power Sources 119-121 (2003) 184.

16. H. Ito, M. Shimakawa, T. Tanaka, and T. Ohzuku, 5th Hawaii Battery Conference, Waikaloa, HI, Jan. 2003.

17. L.A. Chick, L. R. Pederson, G. D. Maupin, J. L. Bates, L.E. Thomas, G.J. Exarhos, Mater. Lett. 10 (1990) 6.

18. L. R. Pederson, L.A. Chick, G. J. Exarhos, US Patent 5114702 (1992).

19. J. Rodriguez-Carvajal, Physica B, 192 (1993) 55., WinPLOTR software downloadable at : http://www-llb.cea.fr/fullweb/winplotr/winplotr.htm.

20. R. Jenkins, in Modern Powder Diffraction, P. H. Ribbe, Editor, The Mineralogical Society of America, Washington, D.C. (1989) Chapter 3.

21. G. T. K. Fey, J. G. Chen, V. Subramanian, and T. Osaka, J. Power Sources, 384 (2002) 112.

22. Y. Gao, M. V. Yakovleva, and W. B. Ebner, Electrochem. and Sol. State Lett. 1 (1998) 117.

23. M. M. Thackeray, C. S. Johnson, J.-S. Kim, K. C. Lauzze, J. T. Vaughey, N. Dietz, D. Abraham, S. A. Hackney, W. Zeltner, and M. A. Anderson, Electrochem. Commun. 5 (2003) 752.

24. J.-S. Kim, C.S. Johnson, and M.M. Thackeray, Electrochem. Commun. 4 (2002) 205.

25. R. Kostecki, personal communication.

Table 1. Unit cell parameters of $LiNi_{1/3}Co_{1/3}Mn_{1/3}O_2$ samples (Space group $R\bar{3}m$), obtained from Full Pattern Matching refinements of patterns in Figure 1. $R_{003/104}$ is the ratio of the integrated intensities of the (003) and (104) peaks.

Final calcination temperature (ºC)	Unit Cell Parameters (Å)		$R_{003/104}$	Average crystallite size,[a] (nm)
	a	c		
GNC,[b] 800	2.861(2)	14.240(12)	0.93	22
600	2.859(3)	14.242(21)	1.00	9
700	2.862(1)	14.255(9)	1.06	18
800	2.861(1)	14.241(9)	1.11	40
900	2.861(1)	14.249(1)	1.16	50
1000	2.861(1)	14.244(3)	1.17	70
Tanaka[c]	2.860(1)	14.228(4)	1.19	70

a. Estimated from Scherrer equation (see text).

b. Sample prepared by glycine-nitrate combustion (see text).

c. Sample provided by Tanaka Chemical Corporation.

Figure Captions

Figure 1: XRD patterns of $LiNi_{1/3}Co_{1/3}Mn_{1/3}O_2$. From bottom to top: samples calcined at 600°C, 700°C, 800°C, 900°C, 1000°C, GNC, and Tanaka samples. Bragg positions are marked as bars and (003) and (104) reflections are labelled. Patterns are offset for clarity.

Figure 2: First cycles of Li/$LiNi_{1/3}Co_{1/3}Mn_{1/3}O_2$ cells at 0.055 mA/cm^2 between 4.3 and 2.5 V. Final calcination temperatures or sample identities are marked.

Figure 3: Discharge capacity as a function of cycle number for Li/$LiNi_{1/3}Co_{1/3}Mn_{1/3}O_2$ cells charged and discharged at 0.055 mA/cm^2 between 4.3 and 2.5 V.

Figure 4: Discharges of a Li/900˚C-$LiNi_{1/3}Co_{1/3}Mn_{1/3}O_2$ cell between 4.3 and 2.5V at various current densities: 1st and 11th discharges at 0.055 mA/cm^2, 2nd at 0.11 mA/cm^2, 3rd at 0.167 mA/cm^2, 4th at 0.22 mA/cm^2, 5th at 0.27 mA/cm^2, 6th at 0.33 mA/cm^2, 7th at 0.39 mA/cm^2, 8th at 0.44 mA/cm^2, 9th at 0.5 mA/cm^2 and 10th at 0.55 mA/cm^2 (approximately C/2.6 rate).

Figure 5: First cycles of Li/900˚C-$LiNi_{1/3}Co_{1/3}Mn_{1/3}O_2$ cells at 0.055 mA/cm^2 charged to 4.3V (○), 4.5V (—), and 4.7V (---). Inset shows discharge capacity as a function of cycle number.

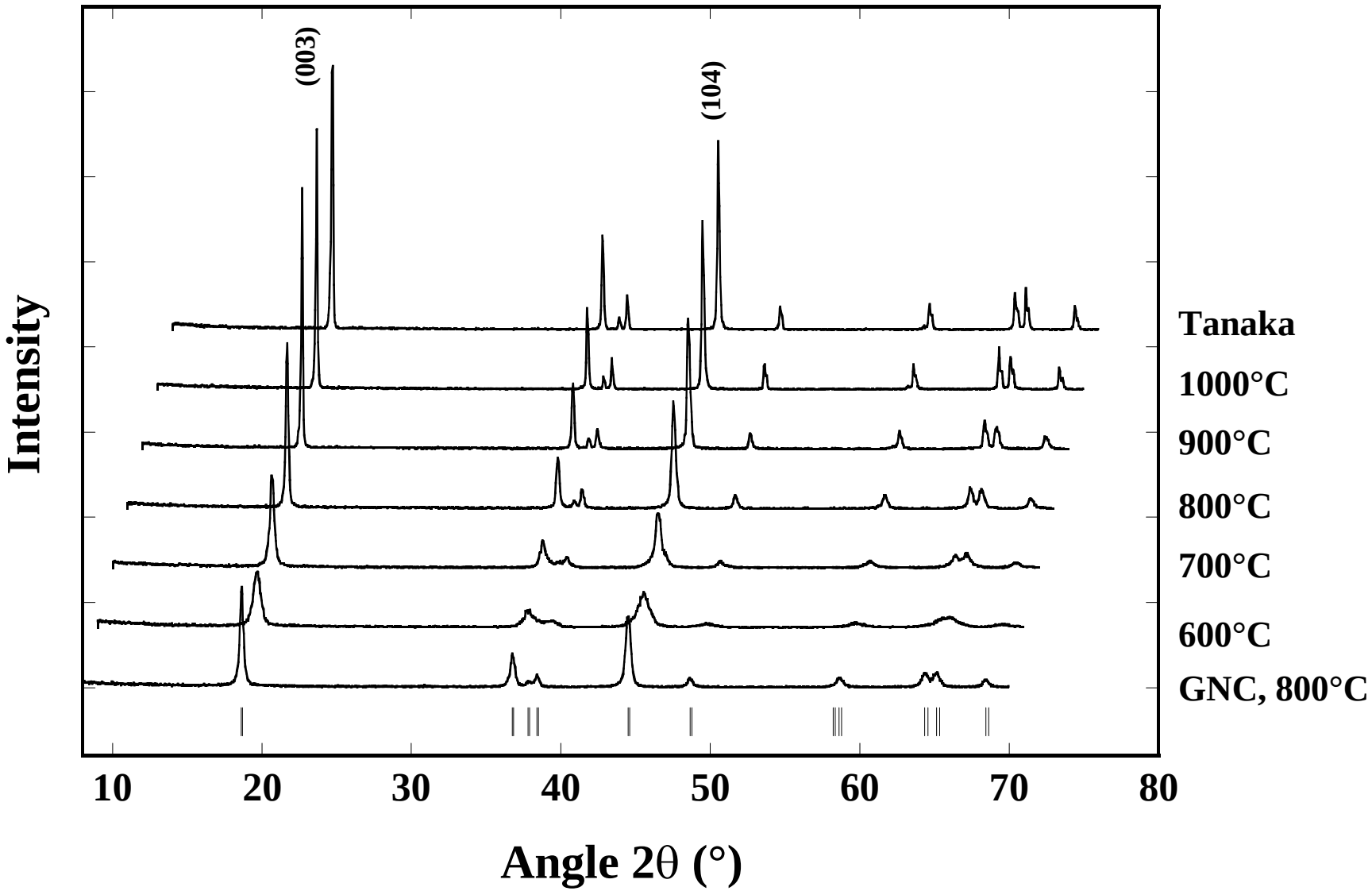
(003)
(104)
Intensity
Tanaka
1000°C
900°C
800°C
700°C
600°C
GNC, 800°C
10
20
30
40
50
60
70
80
Angle 2θ (°)

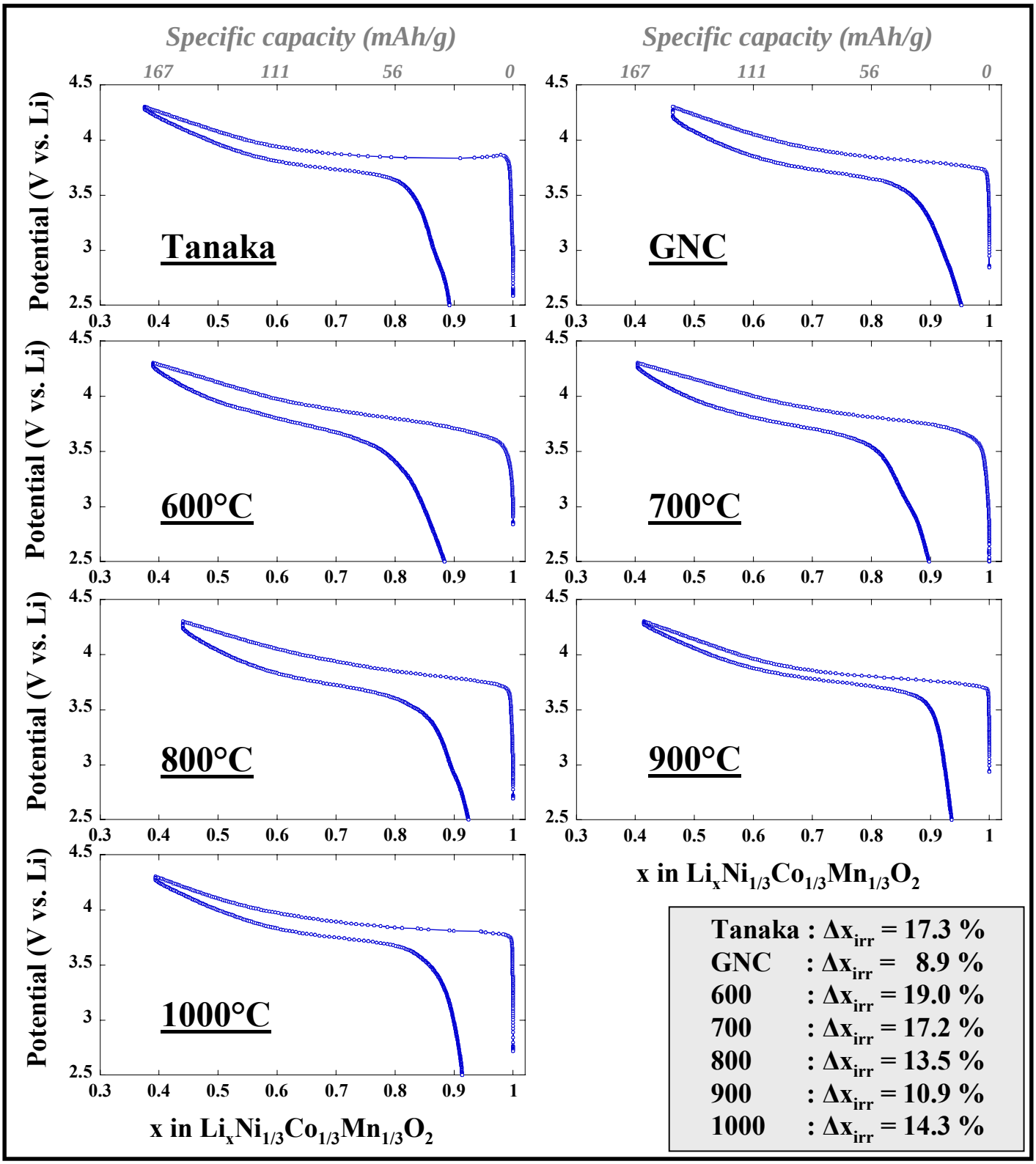
Specific capacity (mAh/g)
167
111
56
0
Potential (V vs. Li)
Tanaka
GNC
600°C
700°C
800°C
900°C
1000°C
x in $Li_xNi_{1/3}Co_{1/3}Mn_{1/3}O_2$
Tanaka : Δx_{irr} = 17.3 %
GNC : Δx_{irr} = 8.9 %
600 : Δx_{irr} = 19.0 %
700 : Δx_{irr} = 17.2 %
800 : Δx_{irr} = 13.5 %
900 : Δx_{irr} = 10.9 %
1000 : Δx_{irr} = 14.3 %

Figure 2

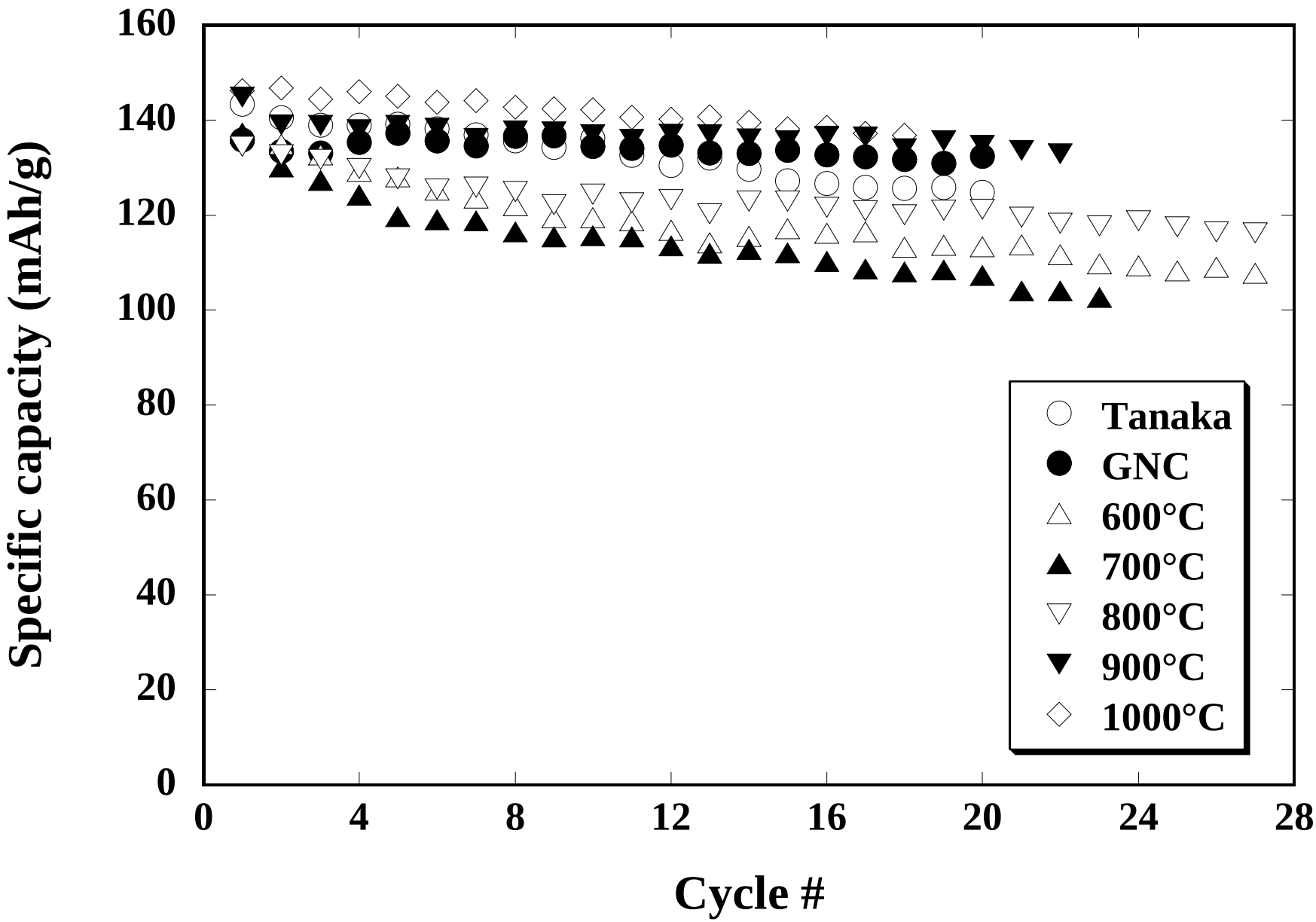
Specific capacity (mAh/g)
160
140
120
100
80
60
40
20
0
0
4
8
12
16
20
24
28
Cycle #
Tanaka
GNC
600°C
700°C
800°C
900°C
1000°C

Figure 3

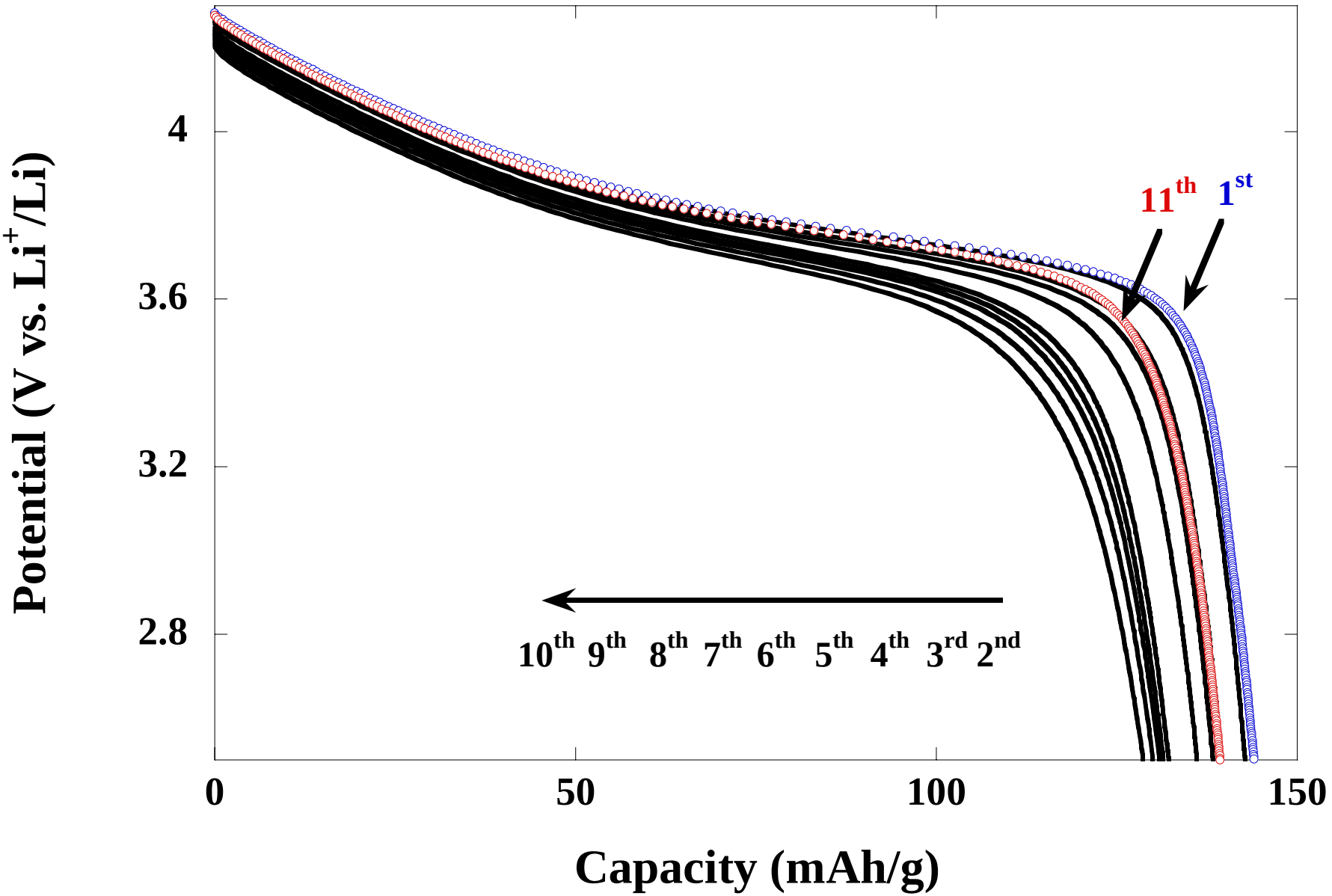
Potential (V vs. Li+/Li)
4
3.6
3.2
2.8
0
50
100
150
Capacity (mAh/g)
11th
1st
10th 9th 8th 7th 6th 5th 4th 3rd 2nd

Figure 4

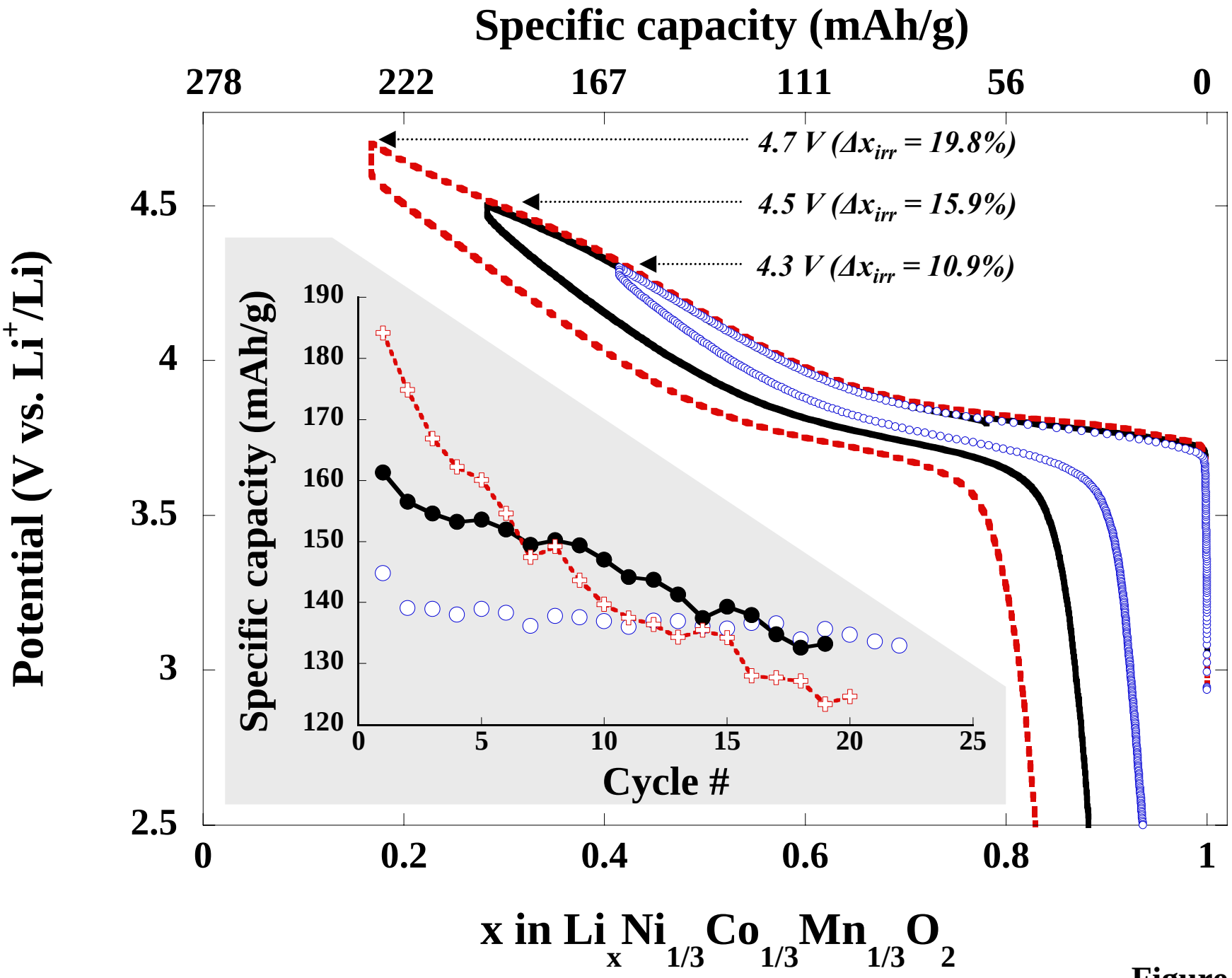
Specific capacity (mAh/g)
278
222
167
111
56
0
4.7 V (Δx_irr = 19.8%)
4.5 V (Δx_irr = 15.9%)
4.3 V (Δx_irr = 10.9%)
Potential (V vs. Li+/Li)
4.5
4
3.5
3
2.5
0
0.2
0.4
0.6
0.8
1
x in Li_x Ni_1/3 Co_1/3 Mn_1/3 O_2
Specific capacity (mAh/g)
190
180
170
160
150
140
130
120
0
5
10
15
20
25
Cycle #

Figure 5